Hyperfine and Host−Guest Interactions of the Mu-Cyclohexadienyl Radical in NaY Zeolite

Donald G. Fleming,*,‖ Mee Y. Shelley,† Donald J. Arseneau, Masayoshi Senba,‡ and James J. Pan§

TRIUMF and Department of Chemistry, University of British Columbia, Vancouver, British Columbia, Canada V6T 2Z1

Emil Roduner

Institut für Physikalische Chemie, Universität Stuttgart, Pfaffenwaldring 55, D-70569 Stuttgart, Germany

Received: February 7, 2002

The adsorption and dynamical behavior of the muonated cyclohexadienyl radical (C_6H_6Mu) in NaY zeolite, formed by muonium (Mu) addition on adsorbed benzene, was investigated by the muon spin resonance (μSR) technique, primarily at loadings of 2−3 C_6H_6 molecules per supercage of NaY. The dynamics of this radical are expected to be the same as its isotopic analogue, C_6H_7, for which there are no similar data available. Both TF-μSR and ALC-μSR spectra were recorded, with the most detailed information provided by the positions and line widths of the avoided level crossing resonances. In concert with ^{2}H NMR, neutron diffraction and molecular dynamics studies of the parent benzene molecule, as well as current theoretical calculations, the dominant adsorption site for the C_6H_6Mu radical is believed to be the S_{II} Na cation, within a supercage, which gives rise to three observed ALC lines, corresponding to *two different orientations* for the muon (proton) of the CHMu methylene group: pointing toward (endo) and away (exo) from the Na cation. The cation interaction gives rise to unprecedentedly large (≈20%) shifts in hyperfine coupling constants, indicative of a strong bond formed with the π electrons of the C_6H_6Mu radical. An additional but weaker resonance line is also seen, which is interpreted as being due to adsorption at the window sites between supercages. The ALC lines associated with the C_6H_6Mu radical bound to both the Na cation and window sites are all broad, ≈1 kG, change little with temperature and exhibit mainly *static* line shapes over the whole temperature range studied, from 3 to 322 K. This indicates a much stronger host−guest interaction for C_6H_6Mu, particularly with the Na cation, than is known for benzene, to the extent that this site acts as an effective *trap* for the free radical, over the critical μSR time scale of 50 ns.

1. Introduction

Zeolites, alumina-silicate microcrystalline materials, possess an almost limitless number of possible structural and/or cation variations.[1,2] They participate in a wide range of industrial separation processes and catalyzed chemical reactions that depend in a complex way on the nature of the adsorbed molecule and its chemical binding within the internal pores and channels of zeolites, and hence on the temperature, loading density, and interactions with the zeolite framework and extraframework cations.[1,3−5] Of the many possible zeolite frameworks, the synthetic "faujasites" have among the largest internal pore volumes, with large α "supercages" of ≈12 Å diameter, accessed by "windows" ≈7.5 Å in diameter. There are 8 of these supercages (SC) per unit cell within which a variety of organic molecules can be accommodated (≈5 C_6H_6/SC at saturation loadings[1,6]), facilitating the use of faujasites, usually in their protonated or transition-metal exchanged forms, as heterogeneous catalysts in the petrochemical industry.[4,5,7,8] A variety of extraframework cations can be incorporated by ion-exchange techniques (to compensate for the anionic framework charge), among which the molecular dynamics of guest iorganic molecules have been most extensively studied in NaX (Si/Al ratio ∼1−1.5) and NaY (∼1.5−3.0).[5,9]

Central to the utility of zeolites as molecular sieves and heterogeneous catalysts is a *microscopic* understanding of the interactions of these guest molecules with the host lattice and with each other. While there have been extensive studies in recent years of molecular adsorption and dynamics in zeolites, the vast majority of these have been for *diamagnetic* molecules, often of benzene and its derivatives.[5,9] It is expected that *paramagnetic* species, either neutral free radicals or radical ions, will also play a role in molecular motion and heterogeneous catalysis in zeolites[3,7,10−14] raising questions as to the nature of the interactions of the unpaired electron within the microcrystalline environment.

The usual technique of choice in the study of free radicals is ESR. While most studies of this nature in zeolites have been of radical cations,[13−17] there are also several reports of ESR studies of *neutral* free radicals in zeolites,[11−13,17−19] some involving stable free radicals.[12,15,19] Radicals are often formed in geminate pairs by photolysis of selected organic precursors, and recombination reactions can be fast, though mitigated by the restricted zeolite geometry at lower temperatures.[11,18,20] Stable nitroxide radicals have also been observed on the *external* surfaces of two MFI zeolites[12] (silicalite and ZSM-5). An important class of neutral organic free radicals are those formed directly by

* Corresponding author. Fax: 604-822-2847. E-mail: flem@triumf.ca.
† Present address: The Schrödinger Corporation, Portland, OR.
‡ Present address: Department of Physics, Dalhousie University, Halifax, NS, Canada.
§ Present address: Smart and Biggar Law Offices, Toronto, ON, Canada.
‖ Alexander von Humboldt Prize recipient, Universität Stuttgart.

10.1021/jp020378e CCC: $22.00
Published on Web 06/05/2002

H-atom addition to unsaturated bonds, which might generally be expected from Bronsted active OH centers in zeolites via specific hydrogen exchange reactions.[21,22] Of particular interest here is H-atom transfer to benzene, leading to the classic cyclohexadienyl radical, C_6H_7, as a basis for more complex aromatic systems in faujasites.[5,7,16,19,23,24] The only report[13] of the direct observation of C_6H_7 in a zeolite, formed by H-atom addition, is from the radiolysis of HZSM-5. However no studies of its dynamics were reported and, to our knowledge, there have been no studies reported at all of this radical in faujasites, where radical recombination is more facile.[18] The observation of transient free radicals necessitates the development of sensitive experimental techniques.

The muonium atom ($Mu = \mu^+ e^-$) is an important microscopic spin probe of the formation, hyperfine interactions and molecular motion of free radicals.[25−27] Positive muons (μ^+) are produced 100% spin polarized, and this polarization can effectively be transferred to a radical by Mu addition reactions, exemplified here by $Mu + C_6H_6 \rightarrow C_6H_6Mu\cdot$, giving the muon analogue of C_6H_7.[25,28−30] The time evolution of the muon spin polarization in the radical can be sensitively monitored by the μSR (muon spin relaxation or resonance) technique, which can be thought of as a variant of magnetic resonance.[31] It has an important advantage over other magnetic resonance techniques, in that it can be utilized to detect essentially *one* radical at a time, and over a wide range of temperatures, obviating concerns about radical recombination reactions.[18]

The present paper is part of a series of detailed measurements of the Mu-cyclohexadienyl radical in faujasites (NaY, NaX, USY, and HY) carried out at the TRIUMF cyclotron over a range of loadings and temperatures and reported here for NaY (Si/Al = 3.4) for below-saturation loadings of primarily 2−3 benzenes/SC. This extends considerably a recent preliminary report of the hyperfine coupling constants for C_6H_6Mu in NaY[32] and complements as well an earlier report in USY at high loadings.[33] Below-saturation loadings faciliate the study of guest−host interactions at distinct adsorption sites in the faujasite, free from phase transitions and other cooperative phenomena that are expected at higher loadings.[5,6,34]

In addition to the fact that there are no previous studies of its isotopic H-atom analogue, the C_6H_6Mu radical was chosen for study in NaY for a number of reasons. First, only one structural isomer is formed, thus eliminating possible ambiguites in interpretation, and it has also been well studied in gases[25] and in the bulk phase.[25,28,29] Second, in addition to USY,[33] the C_6H_6Mu radical has also been studied in other zeolites, notably ZSM-5[30,35] and NaX,[36,37] as well as in silica powders and gels,[38] providing an important basis for comparison with the present data. Third, benzene itself and its molecular dynamics have been extensively studied in faujasites, notably in both NaX and NaY, by X-ray and neutron diffraction,[39−42] by D-NMR,[40,43−47] and by a number of sophisticated Monte Carlo and molecular dynamics (MD) simulations.[9,34, 43,48−52] Finally, and in contrast to NaX,[5,41,53−55] there are only two primary accessible sites for benzene adsorption per SC in NaY, the four equivalent (S_{II}) Na^+ cation sites and the two equivalent window (W) sites, both of which are well established.

2. Sample Preparation

A stainless steel cell of outside diameter 4.1 cm and thickness 1.2 cm was filled with NaY zeolite, obtained from Chemie Uetikon AG of Switzerland (SiO_2/Al_2O_3 mole ratio = 6.8, Si/Al = 3.4, crystal diameter ~2−3 μm) and then sealed with a 25 μm stainless steel welded window of 3.2 cm diameter. This zeolite sample cell was connected to a turbo pump via a copper tube soldered to the cell, dehydrated at high temperature under vacuum, and then loaded with benzene. At these conditions, the framework structure of NaY is preserved on dehydration.[1] A small amount of He heat-exchanger gas was introduced before the copper tubing was sealed using a "cold-weld" crimper (CHA Industries, USA) that produces a vacuum-tight seal. Samples were prepared at least a week ahead of data taking, thereby giving sufficient time for equilibration at low loadings. The bulk of the data reported herein was taken at loadings of 2−3 molecules/SC (mainly at 2/SC), as determined by weight (10−15%) of dehydrated zeolite.

The zeolite sample cell was mounted in a helium-flow cryostat for temperature control, and was then placed in a superconducting magnet that could provide magnetic fields up to 70 kG, aligned with the beam direction. The temperature was varied in the range 3−322 K, and was monitored by three different thermocouples attached to the target cell, which typically gave consistent readings to better than a degree. The spin-polarized surface muons passed through the entrance window and stopped within the zeolite sample, forming the muonated cyclohexadienyl (C_6H_6Mu) radical.

3. Basics of the μSR Technique

High intensity "surface" muon beams were utilized, which are produced ($\pi^+ \rightarrow \mu^+ + \nu_\mu$) with 4 MeV kinetic energies and essentially 100% longitudinally spin-polarized at nuclear accelerators such as TRIUMF, where the experiments were carried out. The time evolution of the muon polarization is manifest by the directional asymmetry seen in the radioactive decay of the muon ($\mu^+ \rightarrow e^+ + \nu_e + \overline{\nu_\mu}$, with a mean life of 2.2 μs) in which the positron is preferentially emitted along the muon spin direction.[31] We have used two different μSR techniques[25,31] to monitor the time evolution of the muon polarization in the C_6H_6-Mu radical: transverse field μSR (TF-μSR), in which the incident muon spin is perpendicular to the field direction, and avoided level crossing resonance (ALC-μSR), where the spin is aligned with the field direction. The TF technique is a "time-differential" one in which the incident muon triggers a counter and starts a "clock", which is subsequently stopped by the detection of a decay positron (or is otherwise reset), and each separate event of this nature is tallied in computer memory. In these experiments, the muon spin was rotated 90° to the beam direction, without the need for any change of sample. In the ALC method, the muon spin is parallel to the applied magnetic field. In this "time-integral" technique, the numbers of decay positrons are recorded in the backward and forward directions (N_B, N_F) while the magnetic field is varied; the asymmetry, or ALC spectrum, is then given by $(N_B - N_F)/(N_B + N_F)$.

3.1. TF-μSR and Muon hfcs for C_6H_6Mu. In TF-μSR the magnetic field causes precession of the muon polarization at frequencies corresponding to transitions between the allowed energy levels characterizing the spin Hamiltonian of a Mu-radical, which in general involves both anisotropic hyperfine and spin−rotation interactions.[26,27,56,57] In isotropic media like gases and liquids, in high transverse fields, Fourier transform TF spectra reveal two characteristic muon precession frequencies for a given radical environment:[25,26]

$$\nu_{R2} = \nu_m + \frac{1}{2}A_\mu \quad \text{and} \quad \nu_{R1} = |\nu_m - \frac{1}{2}A_\mu| \qquad (1)$$

where A_μ is the *isotropic* muon−electron hyperfine coupling constant (hfc) and

$$\nu_m = \frac{1}{2}([A_\mu^2 + (\nu_e + \nu_\mu)^2]^{1/2} - \nu_e + \nu_\mu) \qquad (2)$$

with the Zeeman (Larmor) frequencies $\nu_\mu = \gamma_\mu B$ for muons found in *diamagnetic* environments ($\gamma_\mu = 0.01355$ MHz G^{-1}) and $\nu_e = \gamma_e B$ for the electron ($\gamma_e = 2.8025$ MHz G^{-1}). Single crystals, or random isotropic motion on a short time scale, shorter than the inverse of the hyperfine anisotropy, lead to Lorentzian line shapes. In polycrystalline environments, such as zeolites, Mu-radical precession frequencies can be modified by the angular dependence of the dipolar coupling, which can give rise to TF Fourier spectra of asymmetric shape.[58] Distinct adsorption sites for Mu-radicals can be distinguished if they give rise to hfcs (A_μ) whose difference is greater than the $\sim 1/\tau_\mu \approx 0.5$ MHz frequency resolution of the μSR technique.

An example TF (power) spectrum for the C_6H_6Mu radical in *neat solid* ("frozen") benzene, to be compared with a similar spectrum in NaY (Figure 4, below), is shown in Figure 1, at 263 K. The benzene sample was introduced as a liquid in the same sample cells as used for the zeolite, frozen (in liquid N_2) and then warmed to a given temperature. The relatively sharp radical lines seen are indicative of a largely single-crystal environment. The intense ν_{R1} line at 38.5 MHz is an unambiguous indication that most muons have formed the C_6H_6Mu radical, probably by Mu addition on a short enough time scale (<1 ns) that phase coherence is preserved. The isotropic hfc, $A_\mu = 525 \pm 1$ MHz, is found from the difference of the two radical frequencies (eq 1), and is only about 2% higher than that in the bulk gas or liquid phases.[25]

3.2. ALC-μSR Line Shapes and Nuclear hfcs. Though the clearest observation of a Mu-radical is often provided by TF Fourier spectra (as in Figure 1), this is not always possible, particularly in the case of slowly formed radicals. In the ALC-μSR technique,[26,27] there is no dephasing of the muon spin and Mu radicals need only be formed over a time scale comparable to the 2.2 μs muon lifetime. In the high fields characteristic of this technique, the energy eigenstates of a system that consists of a positive muon (μ^+), an unpaired electron (e^-), and magnetic nuclei (k), are stationary Zeeman states over most of the field range. Crossings of these Zeeman states, at specific magnetic fields where they become near-degenerate, are avoided by the isotropic Fermi contact or by the dipolar interaction of the spins. In these regions, the eigenstates are mixtures of pure Zeeman states, resulting in an oscillatory inversion of the muon spin along the field. A signal appears as a "dip" in the decay asymmetry corresponding to a resonant transfer of muon spin polarization from the backward to the forward direction as the magnetic field is scanned.[25,27] ALC-μSR spectra were acquired at muon rates typically 5×10^5 s^{-1} with about 2×10^7 positrons detected at each value of the magnetic field, which was incremented in steps of about 100 G, depending on conditions. The ALC lines are all broad and superimposed on a slowly varying field-dependent background, which was determined from a computer fit to the asymmetry, as shown below.

There are three different types of ALC resonances corresponding to the magnetic selection rules characterized by ΔM, where $M = m^e + m^\mu + m^k$. The Δ_0 ($\Delta M = 0$) resonance represents the "flip-flop" exchange of spin polarization between the muon and a nuclear spin, and is driven indirectly by matrix elements of the form $S^e_- I^\mu_+$ and $S^e_- I^k_+$, arising from *isotropic* couplings in the spin Hamiltonian.[26,57] This is the only kind of ALC resonance seen in the gas phase[25,59] or in any isotropic environment,[27,28,38] where the dipolar couplings are averaged to zero by fast rotational tumbling. Since these resonances depend primarily on the Fermi contact interaction, transmitted through the σ bonds in the radical, their line positions and widths contain structural information but are generally less informative about molecular dynamics.

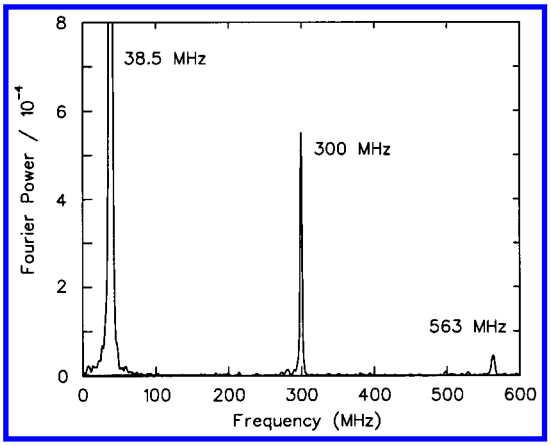

Figure 1. Time-resolved TF-μSR Fourier transform spectrum of pure frozen benzene at a temperature of 263 K and magnetic field of 22.5 kG. It is the Fourier power that is plotted on the ordinate so the signal amplitudes are actually larger than indicated. The two peaks of interest identifying the C_6H_6Mu radical are $\nu_{R_1} = 38.5$ MHz and $\nu_{R_2} = 563$ MHz, the difference being the isotropic muon hfc, $A_\mu = 525$ MHz. The marked reduction in amplitude seen for the ν_{R_2} frequency is due to the limited $\gtrsim 1$ ns time resolution of the apparatus. The large central peak at 300 MHz is due to muons in (unknown) diamagnetic environments.

The Δ_1 ($\Delta M = 1$) "muon flip" transition is induced through the coupling of Zeeman states directly from the *anisotropic* (dipolar) part of the muon hyperfine interaction, arising from matrix elements involving terms such as $S^e_z I^\mu_+$, and is dependent on the angles between the principal axes of the hyperfine tensor and the field direction. Since this tensor has a (body) fixed orientation on the radical, it provides a sensitive means to study reorientation dynamics of that radical. This muon spin flip process is also induced by the operator I^μ_+ in TF-μSR, (e.g., Figure 1), a correspondence that provides an unambiguous identification of a Δ_1 line in ALC-μSR spectra. A further Δ_2 ALC "flip−flip" transition is much weaker,[26] and is of little consequence here.

The positions and widths for both the Δ_0 and Δ_1 resonances provide important information on structure and dynamics of the radical and, in the case of surfaces or crystalline environments, its adsorption site. In the case of the *static* limit of *no* molecular motion, all the components of the hyperfine tensors and their relative orientations are needed to numerically simulate the line shape.[26,60] In a *polycrystalline* environment like a zeolite, a further numerical integration over the angle dependence is also required, to give the proper powder-averaged line shape.

Simulations of powder line shapes for the C_6H_6Mu radical are shown in Figure 2. The top (left) illustrates the Δ_1 resonance for the case of the *static* limit for a rhombic hyperfine tensor with values $B_{zz} = -10.4$ MHz, $B_{xx} = 9.4$ MHz and $B_{yy} = 1.0$ MHz, determined from a durene single-crystal study, corrected for the absence of the methyl substituents.[60] In this simulation the isotropic muon hfc, $A_\mu = 519$ MHz, is typical of that known for C_6H_6Mu in bulk or unperturbed environments[25,30] and corresponds closely as well to a NaY resonance (peak "C") discussed below. In crystalline C_6H_6Mu, one hyperfine component above is close to zero giving an essentially *planar* anisotropy, which accounts for the largely *symmetric* powder shape seen in Figure 2. Note the *width* of this static Δ_1 resonance, which is $\approx \pm 10$ MHz from the dominant hyperfine

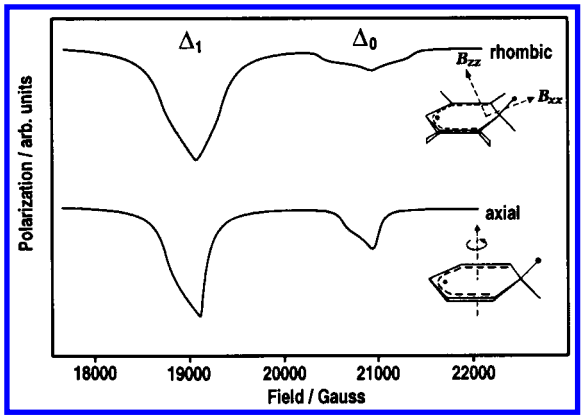

Figure 2. Simulated ALC spectra for the unperturbed C_6H_6Mu radical showing the static case (top) and fast uniaxial rotation limit (bottom) for the Δ_1 and Δ_0 resonances. The parameters of the hyperfine tensors are given in the text. Most relevant to the NaY cases discussed herein are the shapes and widths of the line shapes for a static species, the widths (fwhm) being ≈750 and 1000 G for the Δ_1 and Δ_0 cases, respectively. Adapted from ref 30.

components, or ≈750 G (fwhm). In the analysis to follow, this symmetric shape is fit to a Gaussian, from which the *isotropic* muon hfc, A_μ, is found directly. The position of the Δ_1 resonance then has the same form as in an isotropic environment, given by

$$B_r(\Delta_1) = \frac{1}{2}\left|\frac{A_\mu}{\gamma_\mu} - \frac{A_\mu}{\gamma_e}\right| \qquad (3)$$

The top (right) side of Figure 2 shows the powder simulation for a *static* Δ_0 resonance for the CHMu methylene group of C_6H_6Mu, with the additional components of the proton hyperfine tensor scaled by $\gamma_p/\gamma_\mu = 1/3.184$, and assuming a value for the isotropic proton hfc $A_p = 127$ MHz, also typical of bulk benzene[25] or in siliceous environments.[30,38] The position of the $\Delta M = 0$ resonance has a weak M-dependence for multiple nuclear spins, which can give rise to small shifts, as can the nuclear quadrupole interaction, but in practice these cannot be resolved, and contribute only to a slightly enhanced broadening.[27,35] The Δ_0 powder line shape in Figure 2 is again symmetric and can also be fit to a Gaussian, but in this case the widths (and the positions) depend on both the muon and nuclear hyperfine tensors. For the simulation shown, the fwhm is ≈ 1000 G. A Gaussian fit to the shape is consistent with the most commonly used expression, also adopted herein, for the position of a Δ_0 resonance in isotropic environments,[25,27,28]

$$B_r(\Delta_0) = \frac{1}{2}\left|\frac{A_\mu - A_k}{\gamma_\mu - \gamma_k} - \frac{A_\mu + A_k}{\gamma_e}\right| \qquad (4)$$

with γ_k the gyromagnetic ratio for the nuclear spin. Note that in addition to being broader, the peak *intensity* of the Δ_0 resonance in Figure 2, which in general scales with the product $|A_\mu A_k|$, is much less than for the Δ_1 line.

Fast uniaxial rotation about the axis perpendicular to the plane of the C_6H_6Mu radical partially averages the anisotropy and gives rise to an *axial* hyperfine tensor with components $D_{||} = -2D_\perp = -6.8$ MHz,[26,30] but in this case the powder-averaged line shapes are asymmetric, as shown in the lower part of Figure 2. Both resonances give rise to a cusp-like shape, which is most characteristic for the Δ_1 resonance, with A_μ and $D_\perp$ then found from a numerical fit to the data. Relaxation gives rise to broader (more symmetric) lines of reduced peak amplitude.[29,61] In the case of fast *random* isotropic motion, on a time scale shorter

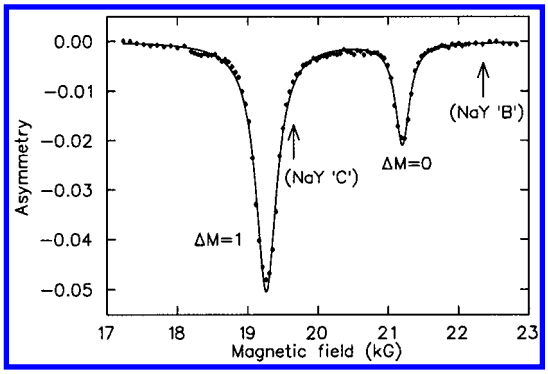

Figure 3. The ALC-μSR (background-corrected) spectrum of the C_6H_6-Mu radical in pure benzene, for the same temperature and conditions as in Figure 1. The solid curves shown are Lorentzian fits. The two strong ALC resonances seen are for the CHMu methylene group and are at characteristic positions for pure (uncomplexed) benzene. The lower resonance at 19.26 kG is the Δ_1 line (≈350 G fwhm) while the upper resonance at 21.21 kG is the Δ_0 line (≈250 G). The relatively sharp lines seen are indicative of a largely single-crystal environment (cf. refs 26, 29), as is the case with the TF Fourier spectrum of Figure 1. The arrows indicate resonance positions found in this field region for C_6H_6Mu in NaY.

than the inverse of the hyperfine anisotropy, $\tau_{ALC} \sim 1/(2\pi D_\perp) \sim 50$ ns for the C_6H_6Mu radical, the Δ_1 resonance averages to zero, leaving only the Δ_0 resonance as an observable, an important signature for molecular motion.[29,61] This feature has aspects in common with D-NMR, where it is the quadrupole tensor, also with a fixed orientation on the molecule, that is averaged out by fast isotropic motion, but in this case on a time scale shorter than the inverse of the quadrupolar coupling constant, $\tau_{NMR} \sim 10$ μs, leading to the collapse of the "Pake doublet".[43,46,62]

Figure 3 shows an example ALC-μSR (background-corrected) spectrum for bulk frozen benzene under the same conditions as in the TF spectrum of Figure 1, to be compared with the NaY spectrum (arrows) of Figure 5 below. In this case the solid lines shown are Lorentzian fits to the data. The widths are considerably narrower than in the simulations shown in Figure 2, indicating, as with the Fourier spectrum of Figure 1, a largely single-crystal environment. A detailed analysis of a similar spectrum has been discussed elsewhere.[26,29] The intense line centered at 19.26 kG in Figure 3 is the Δ_1 muon resonance (not seen in the gas or liquid phases), from which the *muon* hfc, $A_\mu = 524.5$ MHz is obtained from eq 3, the same value as found from the TF spectrum of Figure 1, as should be the case for a Δ_1 transition. It is important to note that this line disappears at the melting point of bulk benzene (278.5 K), in contrast to the present studies of C_6H_6Mu in NaY as well as earlier work on silica gels[38] and other environments.[30,33,35] The transition at $B_r = 21.20$ kG is the Δ_0 resonance due to the proton of the CHMu methylene group, seen also in the gas[25] and liquid phases,[28,63] though at slightly lower fields.[64] From this position, the *proton* hfc in solid benzene is determined, $A_p = 128.2$ MHz at 263 K, from eq 4. For reference, in the gas phase, at a comparable temperature, $A_\mu = 511$ MHz (515 MHz in the liquid) and $A_p = 126$ MHz,[25] only ≈2% changes. There is a hint of a very weak resonance at $B_r \approx 18.3$ kG in Figure 3, which is likely the Δ_2 transition.[26,29]

4. Experimental Results in NaY

4.1. TF-μSR Spectra. A typical TF-μSR Fourier spectrum for benzene in NaY, of several taken at different fields and temperatures, is shown in Figure 4, at a loading of 2 molecules/

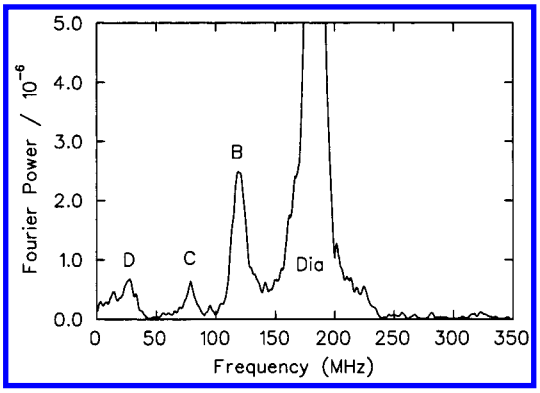

Figure 4. Fourier transform of the C_6H_6Mu radical in NaY loaded with 2 molecules of benzene/SC at a temperature of 322 K and a field of 13.5 kG. The central diamagnetic frequency at 182.8 MHz is off scale in this power spectrum. See also the caption to Figure 1. There are three significant peaks due to the formation of the C_6H_6Mu radical labeled "D", "C", and "B", corresponding to the ν_{R_1} transitions at 32, 78, and 116.5 MHz, respectively. From their peak positions and that of the diamagnetic signal at 182.8 MHz, the muon hfcs can be determined.

SC. In comparison with the TF spectrum of pure solid benzene in Figure 1, where there is only one narrow and intense (ν_{R1}) line below the central diamagnetic frequency, in the NaY spectrum there are *three* such peaks, each much weaker and broader ($\approx$40 μs^{-1}), due to hyperfine anisotropy in this polycrystalline environment.[58] At a loading of 2/SC ($\approx$10% benzene) weaker amplitudes for C_6H_6Mu formation by Mu addition in high TFs are to be expected, in comparison with pure benzene.

The distinct radical peaks of interest in NaY are labeled "B", "C" and "D" in Figure 4, at frequencies 116.5 $\pm$ 3.6 MHz, 78 $\pm$ 3.0 MHz, and 32 $\pm$ 3.5 MHz, respectively. The uncertainties arise from the widths of these weak peaks as well as from systematic differences in peak positions between different histograms and time windows in the Fourier transform. The ν_{R2} transitions, seen weakly in Figure 1, were not observed in NaY. From the measured diamagnetic frequency (182.8 MHz) and eqs 1 and 2, the muon hfcs can be found for each of these peaks: $A_\mu^B = 603$ MHz, $A_\mu^C = 525$ MHz, and $A_\mu^D = 432$ MHz, each with $\approx\pm$5 MHz errors. In the case of the most intense peak, "B", it was possible to fit the time spectrum directly (as in ref 57) giving an overall value for $A_\mu^B = 606 \pm 2$ MHz (322 K), still much less precise than determined by the ALC-μSR spectra discussed below. A few TF runs were also carried out at ambient temperature at much lower fields, where peaks "D" and "B" were of comparable intensity, in contrast to those in Figure 4.

4.2. ALC-μSR Spectra. Figure 5 (top) displays a "raw" ALC-μSR spectrum for C_6H_6Mu in NaY at 322 K, for the same conditions as in the TF-μSR spectrum of Figure 4. The dashed line is a polynomial fit to the field-dependent background of the forward−backward "asymmetry". The arrows indicate the positions of additional (weak) resonances, discussed below. The bottom part of this figure shows the background-subtracted spectrum, revealing *four* clear ALC resonances, in stark contrast with the only *two* ALC lines seen in Figure 3 for bulk solid benzene, where scans over a wider field range revealed no additional peaks.

Figure 6 presents similar Gaussian fits to the (background-subtracted) asymmetry at other representative temperatures within the studied range 3−322 K. The labeling is the same as in the TF-μSR Fourier spectrum of Figure 4, with only peak "A" not common to both. The solid lines in Figures 5 and 6

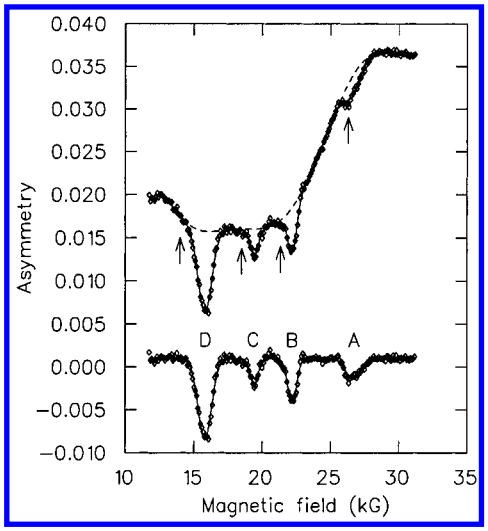

Figure 5. ALC-μSR spectrum of the C_6H_6Mu radical at 322 K, for the same experimental conditions as in Figure 4. Top: the "raw" spectrum. The dashed line represents a polynomial fit to the field-dependent background with the solid curves being global Gaussian fits to the data. The arrows indicate the positions of shoulders or unresolved doublets, confirmed at other temperatures and higher loadings, as well. Bottom: the background-subtracted spectrum showing more clearly the Gaussian fits to the data. Labeling is the same as in Figure 4, with the exception of peak "A", a Δ_0 resonance, in contrast to the Δ_1 resonaces for peaks "D", "C", and "B". Note the largely constant shapes and widths of each resonance as well as the change in these spectra compared to that for pure benzene in Figure 3.

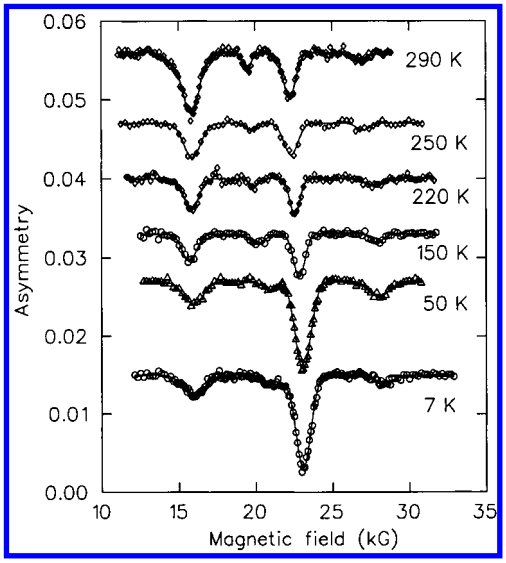

Figure 6. Similar to Figure 5 but over selected temperatures in the range studied (3−322 K). The solid curves are again Gaussian fits with the results recorded in Table 1. The strong *T*-dependence on the amplitudes is of interest, particularly the inverse seen for resonances at $\approx$16 kG (peak "D") and 27 kG ("B"). However, with the exception of the Δ_0 peak "A", the line widths do not change appreciably with temperature and the shapes remain largely symmetrical over the whole temperature range, indicative of the *static* case in the simulations of Figure 3.

are the results of Gaussian fits at each temperature, exhibiting the largely symmetric shapes of each resonance, from which the positions and hence hfcs were accurately determined by eqs 3 and 4. The widths[65] are less precise, being more sensitive to background subtraction, with the amplitudes even more so (not reported). The positions and amplitudes, but generally *not* the widths, of each ALC resonance change with temperature. The results of the fits, giving the resonance positions for C_6H_6Mu

TABLE 1: Line Positions, B_r (kG), hfcs (MHz)[a] and Widths, W (G)[b] for ALC Resonances of C_6H_6MU in NaY

	peak "D"[c]			peak "C"			peak "B"			peak "A"[d]		
T(K)	B_r	A_μ	W	B_r	A_μ	W	B_r	A_μ	W	B_r	A_μ	W
322	15.817(12)	430.7(4)	1040(40)	19.436(10)	529.3(4)	560(40)	22.224(10)	605.2(4)	700(50)	26.618(36)	108.1(13)	1160(120)
290	15.818(30)	431.8(8)	1120(80)	19.497(31)	530.8(8)	490(50)	22.240(16)	605.3(4)	780(70)	26.814(55)	104.9(12)	950(100)
250	15.902(16)	433.0(6)	1160(110)	19.719(38)	536.6(12)	600(90)	22.372(25)	609.5(8)	910(80)	26.906(80)	106.1(16)	≈1000
220	15.820(20)	430.8(8)	980(80)	19.879(40)	541.3(12)	600(100)	22.568(14)	614.5(6)	670(70)	27.5(3)[e]	101.5(40)	≈1000
150	15.778(46)	428.9(17)	1140(130)	20.122(35)	547.9(17)	840(100)	22.833(21)	621.8(9)	725(65)	27.873(90)	102.7(26)	≈1000
50	16.008(28)	436.0(14)	1290(140)	20.675(85)	562.4(16)	≈900[d]	23.049(21)	627.8(6)	1000(70)	28.145(75)	101.9(10)	≈1500
7	16.048(42)	436.8(15)	1130(140)	20.868(65)	568.0(22)	900(200)[d]	23.118(20)	629.3(7)	970(65)	28.35(15)	100.0(25)	1200(200)

[a] Calculated from eq 3 for peaks "D","C", and "B" and from eq 4 for peak "A". [b] "2σ" widths (fwhm = 2.35 σ) from Gaussian fits to the data, as in Figures 5 and 6. [c] Evidence at all temperatures for a broad shoulder peak on the low field side. [d] Indication of doublet structure. [e] Unreliable fit at this temperature.

in NaY and the hfcs, as well as the (2σ) widths for all four resonances, are listed in Table 1. The reported uncertainties include an estimate for reproducibility resulting from separate fits for slightly different fitting conditions as well as an average of small differences in results obtained at different loadings. As noted, most of the measurements were taken at a loading of 2 benzenes/SC, with little or no change in positions or intensities seen in either the TF-μSR or ALC-μSR spectra at a loading of 3 benzenes/SC, consistent with our expectation of measuring guest−host interactions. Additional data taken at a loading of 1/SC gave intensities that generally were just too weak to fit, while at 4/SC, stronger lines were seen, but also sharper additional peaks near "C" appeared, in both the TF and ALC spectra. These additional lines corresponded to a reduced hfc the same as found in bulk benzene at a comparable temperature (Figures 1 and 3, and ref 25), likely due to the presence of extragranular benzene resulting from inadequate sample equilibration at this higher loading.[66]

In comparison with the ALC spectrum of bulk solid benzene in Figure 3, in addition to the fact that there are four clear (symmetric) resonances for C_6H_6Mu in NaY, their *constant* widths with changing temperature (Table 1) are also significant. As in the TF data, the only resonance in NaY which has a similar position, and hence hfc, to that in bulk benzene is peak "C", which represents an important later point for the identification of this peak. Peaks "A" and "D" are somewhat broader (average width ≈1100 G) than "B" (≈ 800 G) or "C" (≈700 G), due to the presence of an unresolved doublet at these loadings in the case of "A" (high-field arrow in Figure 5) and a shoulder on the low-field side of "D" (lowest-field arrow in Figure 5), hinting at additional resonances. There are also indications of additional peaks near "B" and "C" (middle arrows), referred to in ref 32 and commented on further below.

4.3. Site Identification and Peak Assignments. Since, for a given adsorption site, there should only be *two* methylene (CHMu) resonances for the C_6H_6Mu radical (Δ_0 and Δ_1), as in Figure 3, the ALC spectra in Figures 5 and 6 clearly demonstrate that there must be at least two distinct sites or two distinct orientations for the C_6H_6Mu radical in NaY. In analogy with the known sites for benzene in NaY,[5] established by neutron diffraction, D-NMR and MD studies,[40−43,47−49] we consider the (four) equivalent S_{II} Na^+ sites within a supercage and/or the two equivalent (four-shared) W sites between supercages as likely locations for the C_6H_6Mu radical. Since there are twice as many cation as window sites per SC, more intense lines for binding to cation sites are also expected.

4.3.1. The Δ_1 Resonances: Peaks "B", "D", and "C". Since all three of these peaks appear in the TF-μSR spectra (Figure 4), they can immediately be assigned as Δ_1 ALC resonances. The TF evidence, over a range of fields and temperatures, is unambiguous for peaks "D" and "B". Peak "C" is less certain due to its generally much weaker intensity, but the Δ_1 assignment is warranted, supported also by arguments presented below. At 322 K, from the position of the resonant field in Table 1, the muon hfc $A_\mu^B = 605.2 \pm 0.4$ MHz, calculated from eq 3, is the same as the value $A_\mu^B = 606 \pm 2$ MHz found from the TF data discussed earlier, with its much larger errors. Similarly for peaks "D", where $A_\mu^D = 432 \pm 5$ MHz, and "C", where $A_\mu^C = 525 \pm 6$ MHz, from the TF data, in comparison with the much more precise entries at 322 K from the ALC resonances listed in Table 1.

Consider first the muon hfcs for peaks "B" and "D". These are vastly different from the value $A_\mu = 525$ MHz found for solid (single crystal) benzene (at 263 K, Figure 3), well beyond the ≈2% variation in hfc seen for C_6H_6Mu over a range of temperatures in the bulk phase[25] and in other environments.[30,33,36,38] Accordingly, the hfcs A_μ^B and A_μ^D listed in Table 1 for C_6H_6Mu in NaY represent ≈20% shifts in comparison with these other measurements, *unprecedented* for the C_6H_6Mu radical in any environment. This large shift is a clear indication of an unusually strong interaction between the delocalized π electrons of the radical with sites in NaY, most surely with the extraframework S_{II} Na cations. That the C_6H_6Mu radical should be strongly bound to the Na^+ site is expected both from the many other studies of benzene in NaY cited above, with loading conditions similar to those in our experiments, and also from the high calculated binding energy (BE) for benzene at the cation site in NaY, ≈ −80 kJ/mol, depending somewhat on loading,[48,50] a binding much stronger than to the W site,[48,49,51] ≈ −50 kJ/mol. Recent calculations,[67] discussed below, of the BE of the C_6H_6Mu radical to the Na cation give −87.3 kJ/mol, making the radical only slightly more strongly bound than benzene itself.

Since the (four) S_{II} cation sites in a SC of NaY are equivalent, how can one account for *two* distinct muon hfcs, manifest by peaks "B" and "D" here? If the ring were to stay planar, as is the case in the bulk phase,[25,28,68] the muon/proton of the CHMu group at the ipso position would be chemically equivalent and only *one* muon hfc from the methylene group would be observed.[25] However, if the coupling to the Na^+ breaks this symmetry, distorting the ring from planarity, these nuclei would be rendered chemically inequivalent, and two distinct hfcs then become possible. Thus, as indicated in Figure 7, Mu addition to benzene from above the ring to an *exo* position (i.e., opposite the cation) would result in the muon being shifted closer to the center of π electron density,[67−69] giving rise to an *enhanced* hfc, as found for peak "B"; concomitantly, Mu addition from below the ring, forming the endo isomer (peak "D"), would exhibit a *decrease* in hfc, in comparison with the bulk phase. Exactly opposing tendencies should transpire for the corre-

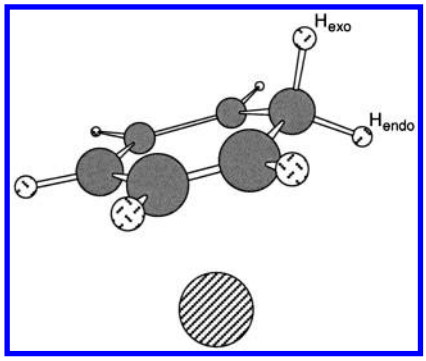

Figure 7. A persepective geometry of the C_6H_6Mu radical due to its interactions with a Na cation (large hatched circle). The ring is tilted with respect to the cation and slightly distorted both at the para and ipso positions, rendering the muon and proton of the methylene group chemically inequivalent. The H_{exo} orientation is closer to the center of π electron density of the ring, thereby *increasing* its hfc relative to the bulk, with just the opposite effect for H_{endo}. Adapted from ref 67.

TABLE 2: Assignments and hfcs for C_6H_6Mu in NaY: Theory and Experiment

	assignment	A_{exp} [MHz][a]	A_{theory} [MHz][b]	dA'_{Exp}/dT [MHz K^{-1}][c]
A	$\Delta_0(S_{II},H_{endo})$	108.1 ± 1.3	106.7	$+0.020 \pm 0.005$
B	$\Delta_1(S_{II},Mu_{exo})$	605.2 ± 0.4	605.6	-0.026 ± 0.001
D	$\Delta_1(S_{II},Mu_{endo})$	430.7 ± 0.4	449.6	-0.006 ± 0.002
	$\Delta_0(S_{II},H_{exo})$	160 ± 5	155.7	n.a.
C	$\Delta_1(W,Mu)$	529.3 ± 0.4	507.4[d]	-0.040 ± 0.002
	$\Delta_0(W,H)$	≈ 130	124.9[d]	-0.013 ± 0.003[d]

[a] hfcs from the experimental results at 322 K, from Table 1, and discussion in the text. [b] Calculated hfcs from the CIS calculations of Webster and Macrae[67] from sodium-induced shifts, at 313 K. [c] Slope of the experimental hfcs with temperature, from Figures 8 and 9. The muon hfcs are plotted in "reduced units", dA_μ'/dT, where $A'_\mu = A_\mu/3.184$. [d] Experimental results for gas-phase C_6H_6Mu at 313 K, from ref 25.

sponding proton Δ_0 resonances, in accord with the recent theoretical calculations of Webster and Macrae[67] (Table 2).

Since the only other sites in NaY large enough to accommodate a benzene molecule are the two (shared) equivalent window sites, we identify peak "C" with the Δ_1 resonance of the CHMu group for the C_6H_6Mu radical bound at this site. Two other aspects of the present measurements support this assignment: First, being far from the nearest Na cation, the 12-oxygen-ring window sites are largely silicious environments, and thus one would expect an essentially unperturbed C_6H_6Mu radical, consistent with the measured values of A_μ^C (Table 1), all similar to data in the bulk phase and other environments (cf. Figure 3). It is important to recognize that peak "C" is *not* in the same place as the Δ_1 resonance for bulk benzene, and peak "B" is even further removed from the bulk's Δ_0 resonance. This is illustrated in Figure 3, the ALC spectrum of C_6H_6Mu in pure benzene, where the positions of the "B" and "C" resonances seen in NaY are indicated by arrows. Since the W environment does not perturb the structure of the C_6H_6Mu radical, it again gives rise to ring planarity and only one muon (proton) hfc. (Also notable is that the average of the hfcs for peaks "B" and "D" is almost the same as the hfc for "C".) Second, at loadings of 2−3 benzenes/SC, the intensities for peak "C" are invariably the weakest, both in the TF (Figure 4) and ALC spectra (Figures 5, 6), consistent with there being only half as many W as S_{II} cation sites. It is also known, from powder neutron diffraction data,[42] as well as IR data,[5] that the occupancy of the W site grows with benzene loadings above 2−3 molecules/SC, suggesting that line "C" should also be more intense in μSR experiments at higher loadings. (Unfortunately, as remarked above, our studies at 4 benzenes/SC revealed additional peaks in the region of "C", which obscured its interpretation.) It is noted that little or no information on benzene at the W site has been provided by D-NMR data, even at saturation loadings.[44]

4.3.2. The Proton Δ_0 Resonances: Peak "A". Since for each muon coupling of the methylene CHMu group a corresponding proton resonance can be expected, there should be *three* partner Δ_0 lines corresponding to the Δ_1 resonances of peaks "B", "D", and "C". The only additional peak clearly evident is "A", which is identified as a Δ_0 resonance by its absence in the TF spectrum of Figure 4. While such a peak, expected at 176 MHz, were it a Δ_1 line, could well be obscured by the tail of the very strong diamagnetic signal in Figure 4, additional TF data taken near 3 kG also revealed no such line. Since there are no additional clear resonances in the region scanned, both the relative positions of the ALC resonances in the solid benzene spectrum of Figure 3 and the simulations in Figure 2, argue in favor of peak "A" being the partner Δ_0 resonance to peak "B". This surmise is supported as well by theory: at 322 K, $A_p = 108.1 \pm 1.3$ MHz, in excellent agreement with the calculations of Webster and Macrae.[67] The experimental assumption here is one of a single (broad) resonance for peak "A", though, as mentioned, this broad structure is partly due to an unresolved doublet, which gives rise to the relatively larger errors assigned to the hfc A_p for this peak in Table 1.

The two additional proton level-crossings expected must be much weaker than peak "A". In the case of the endo muon at the cation site (peak "D"), exhibiting a marked *decrease* in muon hfc relative to the bulk, we can expect the proton in the corresponding exo position to be scaled *up* by roughly the same 20% shift, consistent with the theoretical calculations of Webster and Macrae[67] (quoted in Table 2). Adopting the calculated value of 156 MHz therein gives a resonant field near the shoulder indicated by the lowest-field arrow in Figure 5, at $\approx$14 kG (seen more clearly at a loading of 4/sc). At 290 K, the fitted spectrum shown in Figure 6 gives a field of 14.5 ± 0.2 kG, from which the *proton* hfc, $A_p = 160 \pm 5$ MHz, is obtained from eq 4, with $A_\mu = 432$ MHz. As in the case of peak "A", this Δ_0 resonance is likely quite broad, thus contributing to the width seen for "D", which is consistently broader than "B" (Table 1).

For the radical at the W site (peak "C"), the modest ($\approx$2%) increase in muon hfc noted earlier, indicating a nearly unperturbed electronic structure, suggests a similar weak enhancement for the proton of the methylene group, giving $\approx$130 MHz or an expected Δ_0 resonance at $\approx$21.5 kG near 300 K, indicated by the upper-middle arrow in Figure 5. However, this falls in the tail of the strong "B" line and is difficult to see at this temperature, though it can be discerned as a shoulder in the background-corrected plot (bottom). Better evidence for such a resonance is actually seen in the raw spectra at lower temperatures. That it should be so weak is expected first from the intensity of "C" itself and second from the ratio of intensities shown in the simulations of Figure 2. Additional measurements at higher loadings would aid in the identification of both the Δ_1 and Δ_0 resonances for the C_6H_6Mu radical at this W site.[70]

4.3.3. The Na Δ_0 Resonances. Since both the experimental and theoretical evidence are in agreement that the C_6H_6Mu radical is strongly bound to the Na cation, there should also be *two* Δ_0 resonances due to the *sodium* ($I = 3/2$) nuclear hyperfine couplings, arising from the muon couplings at peaks "D" and "B". Such Δ_0 nuclear resonances have been observed from μSR studies in Cu- and Na-exchanged ZSM-5,[30,35] giving rise to

additional strong, broad lines not seen in cation-free (silicious) ZSM-5. Though calculations are underway,[67] there are as yet no reported values for the Na hfc expected from the binding of the C_6H_6Mu radical to the cation in NaY.

In Cu-ZSM-5 the nuclear hfc was found to be 161 MHz, corresponding to a spin population transfer to the Cu cation of 2.7%.[30] In a recent ESR study of the Li-phenalenyl radical in Y-zeolite the measured isotropic hfc of 59 MHz (sign undetermined) corresponds to a 16% spin transfer to the Li ion.[19] In the calculations of Webster and Macrae, the effective charge on the Na, due to its binding with the C_6H_6Mu radical, is 0.88,[67] which suggests a comparable spin transfer of 12%, neglecting lattice contributions. Assuming the same value for the spin transfer to Na from the C_6H_6Mu radical in NaY as measured in the Li−Y study of ref 19, would correspond to $A_{Na} = 148$ MHz, similar to the measured value in Cu-ZSM-5. However, since the *intensity* of a Δ_0 resonance scales as $|A_\mu A_k|$, and it is unlikely that there are additional strong resonances outside the wide region scanned, we surmise that $A_{Na} \ll 161$ MHz for C_6H_6Mu in NaY. Possible candidates here are the additional or doublet structures near peaks "C" and "A" commented on earlier, most evident for "A", indicated by the arrow in Figure 5 at ≈26.3 kG. If this were the sodium Δ_0 resonance paired with peak "B" ($A_\mu^B = 605$ MHz, Table 1), then inserting $\gamma_{Na} = 0.0832\gamma_\mu$[71] into eq 4 yields an expected hfc of $A_{Na} \approx -50$ MHz. This same value associated with the endo muon of peak "D" would give a second Δ_0 resonance at ≈19.2 kG, near peak "C", but somewhat shifted from where an additional weak structure at ≈18.5 kG can almost be seen (lower-middle arrow in Figure 5), which is again somewhat clearer at lower temperatures (at ≈18.7 kG at 50 K). A resonant field of 18.5 kG gives $A_{Na} \approx -30$ MHz. Since appreciable shifts in the position of weak peaks can result from errors in background subtraction, these arguments only provide a very rough (average) estimate for $A_{Na} \approx -40 \pm 10$ MHz. The large *negative* value is somewhat surprising and may indicate spin polarization through the radical-ion bond and/or additional interactions with the zeolite lattice, but this can only be confirmed by detailed calculations as well as by additional data at higher loadings.

5. Discussion and Comparison with Theory

5.1. Muon and Proton hfcs. *5.1.1. Room Temperature.* A hyperfine coupling constant gives a measure of the electron spin density on a nucleus and correspondingly depends on the geometric structure of the radical. The equilibrium geometries of both the unperturbed (and unsubstituted) cyclohexadienyl radical (C_6H_7) and its Mu analogue are known to consist of a planar 6-carbon ring, given by the nodal plane of the π-system, established by high level ab initio calculations.[67−69] The unpaired electron in the radical occupies an MO derived from the 2p atomic orbitals centered at the ortho and para carbons together with 1s orbitals from the H atoms of the CH_2 group.

The most recent calculations by Webster and Macrae of the hfcs for both the unperturbed radical and the effect of its interactions with a Na cation, have utilized the "CIS" (configuration interaction singles) method of Chipman.[67,68] The cation is not ring-centered in these calculations but shifted closer to the para-carbon, which has the effect of distorting the ring from planarity. As profiled above, this distortion, also affecting the C-6 (ipso) carbon, due to an additional steric effect, tilts the p-orbital centered on the para-carbon closer to the methylene proton at the exo position, with the opposite effect at the endo proton, as indicated in Figure 7. The reduction in symmetry, rendering the methylenic protons chemically inequivalent, translates into a 30.8 MHz *increase* in hfc at the exo position with a corresponding *decrease* of 18.2 MHz at the endo position.[67] For comparison with the μSR results, the "reduced" muon hfc, $A'_\mu = A_\mu\gamma_p/\gamma_\mu = A_\mu/3.184$, is introduced, which corrects for the uninteresting isotopic ratio of magnetic moments. Thus, A_p and A'_μ should be the same in the absence of any dynamic isotope effects. In comparison with the experimental results reported for the (planar) C_6H_6Mu radical in the gas phase[25] (at 313 K), these *same* CIS-calculated shifts give values of $A'_\mu = 190.2$ MHz (exo) and 141.2 MHz (endo) with the corresponding proton hfcs predicted to be 106.7 MHz (endo) and 155.7 MHz (exo). It is noted that A'_μ for the endo muon is actually *less* than A_p for its proton counterpart, a first-time situation for the C_6H_6Mu radical. The full calculated muon (and proton) hfcs for the cation-bound radical are given in Table 2, and compared therein with the experimental assignments. The calculated values, though "normalized" by the gas-phase μSR data, assume no further isotopic effect on the muon hfc, but nevertheless are in *remarkably* good agreement with the present experimental results at 322 K (slight corrections for the small difference in temperature actually improves this agreement). The *slopes* of the hfcs with temperature, dA/dT (A'_μ for the muon), are discussed separately below. Since there are as yet no theoretical calculations for the window site, comparisons with "theory" in Table 2 are with the gas-phase data,[25] consistent with the assumption of an unperturbed radical.

In the one measurement of the hfc of the C_6H_7 radical in a zeolite, by radiolysis-induced H-atom addition to benzene in HZSM-5,[13] the reported hfcs for the methylene (and ring) protons are essentially the same as in the bulk (liquid) phase, $A_p = a(CH_2) = 48$G (134 MHz) (see also ref 25), demonstrating little or no distortion of the ring due to its interactions with the HZSM-5 framework, in marked contrast with the present μSR results in NaY. The observation of undistorted C_6H_7 in HZSM-5 is consistent, though, with the μSR measurements of C_6H_6Mu in other environments, as noted above, where A_μ differs from its bulk value by only 2%.

5.1.2. Temperature Dependence. Additional information on molecular or conformational structure of free radicals can be provided by a study of the temperature dependence of their hfcs. This is well established in μSR studies of alkyl radicals, where rotation about the C−C bond effects large changes in muon coupling,[26,27,72] due to an effective lengthening of the C−Mu bond compared to C−H, resulting from zero-point vibration in an anharmonic potential.[73] The temperature dependence of both the CHMu group as well as the ring protons of C_6H_6Mu in the bulk phase has also been studied by μSR (more so, in fact, than by ESR).[25,28] In the bulk (also solid, Figure 3) phase, A'_μ is about 20% higher, while A_p is about 10% lower, at the ipso position, compared to the ESR value for the C_6H_7 radical and both $A'_\mu(T)$ and $A_p(T)$ *decrease* with increasing temperature. Zero-point effects impact here on the hyperconjugation mechanism affecting the spin population at the methylenic position arising from the π network, leaving, on average, more electron spin density on the Mu atom.[26,28,67−69] Isotope effects of this nature are quite significant, which suggests that the generally excellent agreement between theory and experiment seen in Table 2, where these effects have not been explicitly considered, may be somewhat fortuitous.

There are as yet no theoretical calculations published of $A_\mu(T)$ or $A_p(T)$ for C_6H_6Mu, either for the isolated species or for its interactions in NaY, though both are anticipated from the ongoing calculations of ref 67. The present experimental results for $A'_\mu(T)$ and $A_p(T)$, from the entries in Table 1 (including as

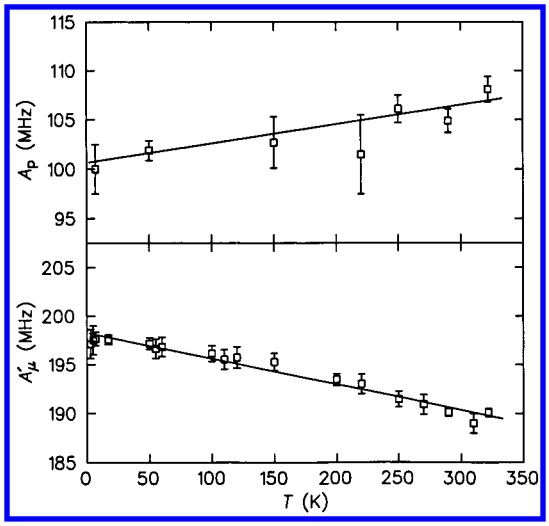

Figure 8. The temperature dependence of the isotropic hyperfine coupling constants for the exo muon position of the CHMu group, A_μ'(B) *(lower)*, and endo proton, A_p(A) *(upper)*, arising from the coupling of the C_6H_6Mu radical to the cation site in NaY. The muon hfc is plotted in "reduced units", $A_\mu' = A_\mu/3.184$. The solid lines are straight line fits and yield the slopes $dA_\mu'/dT = -0.026 \pm 0.001$ and $dA_p/dT = +0.020 \pm 0.005$ MHz K^{-1}, respectively. The slope of $A_\mu'(T)$ is much the same as measured in the bulk phase,[25] but that for the proton hfc has the *opposite* slope, and is taken as evidence for distortion of the ring from planarity, in accord with current theoretical calculations.[67]

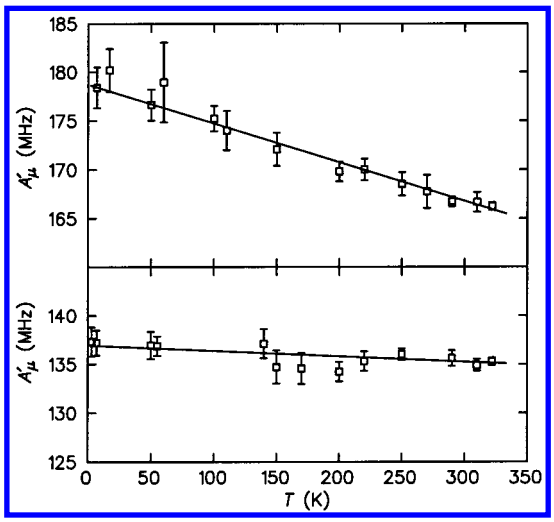

Figure 9. The temperature dependence of the muon isotropic hfcs $A_\mu'(T)$ for the C_6H_6Mu radical at the W site (peak "C", *upper*) and for the muon of the CHMu group in the endo position at the cation site ("D", lower), the opposite orientation to that in Figure 8 (bottom). The straight line slope yields $dA_\mu'/dT = -0.006 \pm 0.002$ MHz K^{-1} for the endo muon, a shallow but still negative slope. The slope at the window site is the most negative yet seen for the C_6H_6Mu radical, $dA_\mu'/dT = -0.040 \pm 0.002$ MHz K^{-1}.

well additional data for A_μ') are shown in Figures 8 and 9. Figure 8 plots these values for the Na-bound radical with the Mu in the exo position (lower plot) and for the corresponding endo proton (upper), superseding a preliminary analysis in ref 32. Figure 9 (lower) presents the analogous plot for the Mu in the endo position but in this case the upper plot is for $A_\mu'(T)$ from the *window* site. In both figures the solid lines are linear fits to the data, giving the slopes of interest, in the last column of Table 2.

In the bulk (gas[25] and liquid[28]) phases the slopes for both $A_\mu'(T)$ and $A_p(T)$ are similar both to each other and within phases, indicating only a minor perturbation of the electronic structure affecting the CHMu group: $dA_\mu'/dT = -0.025$ MHz K^{-1} (liquid) and -0.020 ± 0.002 MHz K^{-1} (gas), with $dA_p/dT = -0.012$ MHz K^{-1} (liquid, similar to the ESR value,[74] -0.018 MHz K^{-1}) and -0.013 ± 0.003 MHz K^{-1} (gas). No T dependence in hfc was detected for the ring protons, and though the values are much smaller, this has been interpreted as evidence for a rigid ring structure, consistent with measurements of the ^{13}C isotopomer by Yu et al.[28] These authors have surmised that the observed T dependence of the muon and proton hfcs in the bulk is primarily due to an out-of-plane "wagging" motion of the methylene group. On the other hand there are 33 normal modes and all contribute with differing degrees and signs to the temperature dependence, requiring a complete calculation of the proper Boltzmann average of vibrational states.[67]

The situation for the C_6H_6Mu radical in NaY is dramatically different from the bulk[25] in several respects, as the plots in Figures 8 and 9 make clear. In addition to the aforementioned 20% shifts in hfcs for the cation-bound radical, the slopes at both the cation and window sites exhibit markedly different behavior (Table 2). Thus, while for the exo muon, $dA_\mu'/dT = -0.026 \pm 0.001$ MHz K^{-1} is essentially the same as found in the bulk phase (and in NaX[36]), in contrast, $A_p(T)$ for the corresponding endo proton at this site *increases* considerably with increasing temperature, $dA_p/dT = +0.020 \pm 0.005$ MHz K^{-1}, the *first* time this *opposite T* dependence has been seen for the C_6H_6Mu radical. Were the ring planar, we would expect to see the same slopes as in the bulk phase. However, because of the distortion from planarity arising from binding to the cation, qualitatively, with increasing temperature, the muon in the exo position tends to move further away from the center of π electron density at the ortho and para carbons, with the endo proton exhibiting just the opposite effect,[67,68] giving rise to a concomitant change in the (σ-bond) spin density, *decreasing* $A_\mu'(T)$ while *increasing* $A_p(T)$. To our knowledge, the only other example of a positive slope for the proton hfcs with temperature for the cyclohexadienyl radical is from the early work on silyl and other electropositive substituents by Kira et al.,[74] also attributed to distortions from ring planarity. Additional support for the existence of a distorted C_6H_6Mu radical, claimed here, is provided by recent data on radical intermediates formed by hydrogenation and dehydrogenation of cyclohexenes on Pt surfaces, studied by surface vibrational spectroscopy.[75]

The comparisons in Figure 9 are no less dramatic. The temperature dependence of $A_\mu'(T)$ for the muon in the endo position (peak "D") displays a very shallow, albeit still *negative* slope: $dA_\mu'/dT = -0.006 \pm 0.002$ MHz K^{-1} (lower plot). Since this has the same orientation as the proton in Figure 8, one might naively have expected a similar (positive) slope, the pronounced difference seen indicating then the importance of differing dynamic isotope effects. This comparison alone strongly suggests that it is not just the motion of the CHMu group that is responding to changes in temperature but is some concerted response of all active normal modes, likely including as well the temperature dependence in the Na-ring binding interaction itself, and possibly with the zeolite framework at large. If the latter interaction(s) were sufficiently positive they might well largely offset the inherently negative temperature dependence observed for the unbound radical in the bulk phase.[25]

The overall complexity of these temperature-dependent interactions for C_6H_6Mu in NaY (and the limitations of simplistic models) is further revealed by the dependence of $A_\mu'(T)$ for the radical at the W site in Figure 9 (upper plot).

Since the hfcs suggest a nearly undistorted (planar) structure at this site, it is reasonable to expect the same T dependence as in the bulk, but in fact the slope seen in NaY, $dA'_\mu/dT = -0.040 \pm 0.002$ MHz K^{-1}, is almost twice that seen in the bulk.[25] It is correspondingly much steeper as well in comparison with that for the exo muon in Figure 8, suggesting perhaps freer motion involving different normal modes than are involved for the radical bound at the cation site, possibly involving interactions with the framework Al ions. Fitch et al. though, in their now-classic neutron powder diffraction study of benzene in NaY,[42] concluded that there was more restricted motion at the W site, which indeed might be expected from the H-bonding of the ring protons with the O-atoms at this site, established from IR data.[5]

5.2. Aspects of Dynamics. *5.2.1. ALC Line Shapes.* In principle, the same information about line widths and dynamics can be obtained from both the TF (Figure 4) and ALC spectra (Figures 5, 6), but in the present study the TF Fourier peaks are too weak and broad to give quantitative information, so the discussion of dynamics here is based on the ALC line shapes alone. As outlined earlier, the widths of the Δ_0 resonances are less sensitive to reorientation dynamics in polycrystalline or surface environments since this resonance is also visible under isotropic conditions. More sensitive are the Δ_1 resonances, because reorientation faster than the time scale set by $\tau_{ALC} \sim 50$ ns for C_6H_6Mu partially or completely averages out the hyperfine anisotropy, giving rise to motionally narrowed regimes that directly impact on both the presence and shapes of the Δ_1 lines. This feature has aspects in common with D-NMR, but on the much longer time scale of $\tau_{NMR} \sim 10$ μs. Partial averaging of the hyperfine anisotropy, due to fast motion about a preferred axis (uniaxial rotation for C_6H_6Mu), gives rise to the asymmetric shape of the *axial* powder pattern (lower panel of Figure 2), in contrast to the symmetric shapes seen for the *static* limit (upper panel). In D-NMR the corresponding situation is the observation of a Pake doublet with reduced quadrupolar splitting. For fast but *random isotropic* motion, the Δ_1 transition disappears in the μSR case, due to complete motional averaging,[26,29,30,61] whereas in the parallel situation in D-NMR, the Pake doublet collapses to a single line.

The observation of three clear Δ_1 resonances, even at 322 K (Figure 5), is unambiguous evidence that there can be no fast random jumps of the C_6H_6Mu radical between tetrahedrally related sites on the μSR time scale of ~50 ns—otherwise such resonances would disappear in this cubic-symmetry material. It is interesting to note that in the aforementioned ESR study of the Li-phenalenyl radical in Y-zeolite, which exhibits a large (axial) hyperfine anisotropy, the ESR signal disappears above 17 K, and, moreover, no signal was seen in NaY,[19] suggesting some form of dynamic disorder, not found in the present μSR study of the C_6H_6Mu radical. The Δ_1 lines in NaY are all much broader than in the gas or liquid phases[25] and considerably broader as well than seen in the single-crystal environment for solid benzene in Figure 3. In comparing the line shapes of Figure 2 for (fast) uniaxial motion of the C_6H_6Mu radical (bottom panel) with the shapes of the experimental resonances seen in NaY over the range of temperatures studied (Figures 5, 6), it is apparent that the experimental lines are much more symmetrical than axial powder shapes, consistent with the Gaussian fits shown. Moreover, the widths, slightly broader for peak "D" while narrowest for peak "C" (as discussed earlier), do not vary much with temperature (Table 1). There might be some motional narrowing effects on a time scale $\ll \tau_{ALC}$, reflected in the somewhat narrower lines seen at the higher temperatures for peaks "B" and "C" (Table 1), but of insufficient amplitude to appreciably alter the static line shapes. By and large all three Δ_1 peaks are either broader than or tend to exhibit the *static* line widths (≈750 G) seen in the (top left) panel of Figure 2, over the full range of temperatures studied.

This conclusion is supported as well by the shape of the Δ_0 resonance, due to the proton hyperfine coupling of the cation-bound radical (peak "A"). The line shapes are again symmetric, independent of temperature, and of essentially constant width, also consistent with the simulations in Figure 2 (top right) for a rigid radical, of fwhm ≈ 1000 G.

The argument that the cation-bound resonances ("A", "B", and "D") have the full static widths shown in Figure 2 relies on the assumption that the C_6H_6Mu radical, when bound to the Na^+, has essentially the same hyperfine anisotropies as the free radical. Since geometric distortions are small (ref 67 and Figure 7) and anisotropies reflect the spatial distribution of the unpaired electron as seen from a nucleus, this assumption is reasonable, pending detailed calculations. The large changes in the isotropic couplings seen for C_6H_6Mu in NaY will simply shift the positions of the resonances, without affecting the widths. In fact, the simulations shown in Figure 2 are almost the correct parameters for peak "C", in the silicious environment at the W site. This peak does appear to be somewhat narrower than "B" (Table 1) and may represent the correct static limit at the lower temperatures for the unperturbed radical.

The conclusion that the C_6H_6Mu radical remains essentially immobilized at the S_{II} cation over the whole temperature range studied (3−322 K), indicates a high activation energy for motional effects, even for in-plane rotations, as well as a relatively strong BE of the radical to the cation site.[67] That there appears to be essentially *no* motion of the C_6H_6Mu radical bound to cation sites in NaY was a surprising result and suggests that the extraframework cations act as effective *traps* for this radical over the characteristic ~50 ns time scale probed by the μSR technique, at least up to temperatures of 322 K (55 °C). This result for NaY is in *marked contrast* to the situation seen in μSR studies of silicious ZSM-5, where the absence of cations means that the ALC line widths for both the Δ_1 and Δ_0 CHMu resonances change by an order of magnitude over a comparable temperature range and also where clear evidence for uniaxial rotation is seen.[30] The results of the present study are also completely different to earlier ALC-μSR studies of C_6H_6Mu at high loadings in USY,[33] where in contrast to NaY, only *two* resonances were seen (as in the bulk phase, Figure 3, and in silicious ZSM-5), but with dramatic differences in line-widths, indicating large-amplitude motional effects. Other ALC-μSR studies of C_6H_6Mu in cation-exchanged ZSM-5[30,35] show *three* clear resonances, also with dramatic differences in widths compared to the present NaY results. Comparisons of this nature provide a convincing demonstration of the sensitivity of the μSR technique to different zeolite environments.

The present NaY results of a static radical appear, at first glance, to be in sharp disagreement with another TF-μSR study (only) in faujasites, where evidence for diffusional motion of C_6H_6Mu over the temperature range ~190 to 270 K has been reported in NaX,[36] with similar results seen in related faujasites.[37] There are, however, two principal differences. First, the latter studies appear to have been carried out at high or uncertain loadings, near (or above) saturation, suggesting that what was observed also involved appreciable guest−guest interactions. Second, NaX-type zeolites have additional cation (S_{III}) sites that can accommodate benzene[41,53−55] and it could be that these additional sites are preferentially populated. Indeed, our own preliminary results from ALC-μSR studies in NaX indicate very

different results to NaY, with only two clear resonances seen, closer in fact to the observations in silicious ZSM-5 or even in the bulk phase.

Finally, a comment here on the changing intensities of peaks "B" and "D" with temperature, seen in Figure 6. If the ring were bound symmetrically to the Na^+, one might expect exo Mu addition to be more facile, i.e., giving enhanced intensity for peak "B". However, near ambient temperature, peak "D" is actually more intense (Figure 5) with "B" growing in apparent intensity with decreasing temperature (Figure 6). That peak "D", which we have argued arises from endo Mu addition, should be so intense at the highest temperatures, suggests that the effect of the Mu addition is to shift the Na toward the para-carbon, as predicted by the calculations of ref 67. Still the changing intensities of these two peaks with temperature are puzzling. This appears to be more of a thermodynamic than a kinetic effect, with the ALC intensity being qualitatively proportional to the equilibrium constant for binding of the C_6H_6Mu to the cation. While some interconversion of "B" (exo muon) to "D" (endo) with increasing temperature is perhaps possible, for example by a "ring flip", this would surely involve a high activation energy, $\gtrsim$ 15 kJ/mol, judging by MD simulations for a similar ring flip of benzene,[48,49] as well as being mitigated against by the relatively strong BE of the radical to the cation.[67] Moreover, were this to occur, we would expect increased line widths for "B", not seen in the data (Table 1). (It can also be noted that any out-of-plane 2-fold rotation on a fast enough time scale would be inconsistent with the observation of distinct Δ_1 resonances.) That "D" appears to be most intense at the higher temperatures suggests that the changes in vibrational entropy, ΔS, accompanying the muon addition process, have the opposite signs for the exo and endo isomers, with ΔS more negative for the exo configuration. At the same time, both ΔS and ΔH may well be T-dependent and there may also be small changes in ΔH for the addition step in these two different orientations, both of which will need to be addressed by detailed theoretical calculations.

5.2.2. Comparison with D-NMR Data and MD Simulations. The present results demonstrating a *static* C_6H_6Mu radical at the cation site are also at variance with what is well-known for benzene itself in faujasites (NaY and NaX) from D-NMR[43,44−46,76] and MD simulations.[9,48−52] The simulations of ref 48 give an activation energy (E_a), for axial (in-plane, hexad) rotational motion $\approx$ 1 kJ/mol at the cation site with corresponding correlation times $\tau_c \sim 1$ ps near room temperature. These same calculations indicate that the (out-of-plane) rotation resulting from *intra*-cage motion between different S_{II} sites, has a much higher activation energy, $\approx$15 kJ/mol, and correspondingly a much longer correlation time, $\gtrsim 1$ μs near room temperature. From the D-NMR data it is well-known that in-plane rotation is very fast on the ~ 10 μs NMR time scale, with an experimental E_a found to be 2−5 kJ/mol.[40,76] From the parameters given in ref 76, $\tau_c = 10.5$ ps at 300 K, in qualitative agreement with the MD simulations of Klein et al.[48] Correlation times of this order are fast on *both* the μSR and NMR time scales. Were the same conditions to prevail for the C_6H_6Mu radical in NaY, we would surely see axial powder lines, reinforcing the claim here of static line shapes. This in turn suggests that the E_a for in-plane motion of C_6H_6Mu is $\gg$ 1 kJ/mol, perhaps largely due to the strong electrostatic interaction between the Na cation and the radical. The strong localized interaction of the C_6H_6Mu radical is also indicated by its distortion from ring planarity.

At low loadings benzene also undergoes isotropic diffusional motion above room temperatures in NaY, with jump times that remain fast on the NMR time scale ($\tau_c \gtrsim 10$ ns), as evidenced by collapse of the Pake doublet.[40,43,46,47] Jump times of this order would be much slower on the μSR time scale though, comparable to τ_{ALC}, and would also lead to marked deviations from static ALC line shapes (seen, for example, in ZSM-5[30]), again inconsistent with observations for the C_6H_6Mu radical in NaY.

In addition to its somewhat higher BE to the cation,[67] due to its open shell structure, in comparison with benzene,[48,49,51] the C_6H_6Mu radical also does not have the 6-fold symmetry of benzene, so one might well expect larger rotational barriers. Effects of this nature have been seen in simulations of in-plane rotation for *p*-xylene at the cation site in NaY,[77] giving a 10-fold higher activation energy than for benzene,[48] with an even higher out-of-plane barrier of $\sim$30 kJ/mol. The hindered in-plane rotation of the *p*-xylene, compared to benzene, due presumably to the steric interaction of the methyl groups, has also been observed experimentally.[23]

6. Summary and Prospects

We have investigated the adsorption and dynamical behavior of muonated cyclohexadienyl radicals in NaY zeolites, using the FT-μSR and ALC-μSR techniques, over a range of loadings but primarily at 2 molecules of benzene/ SC, where guest−host interactions are expected to dominate. Our purpose in studying C_6H_6Mu was to obtain information about the dynamical behavior of the ordinary C_6H_7 radical in faujasites, which may be regarded as a prototypical neutral cyclic (aromatic) radical in these systems, of general interest to the petrochemical industry.[7,8] There appears to be only one ESR measurement of C_6H_7 (in ZSM-5[13]), but no other information on molecular dynamics is available. As such the present paper, taking advantage of the high sensitivity of the μSR technique, makes an important contribution to the study of *neutral free radicals* in faujasites.

Both the unprecedented magnitudes of the shifts seen and particularly their *opposite* temperature dependences, $A'_\mu(T)$ and $A_p(T)$, negative for the exo muon and positive for the endo proton (Figure 8), are taken as evidence for a strong interaction of the C_6H_6Mu with the Na cation, favoring a bent-ring structure of this adsorbed radical over the normal planar structure. The observation by μSR of a radical distorted by interactions with extraframework cations in the zeolite is the first report of its kind in these systems, and could be a first step in identifying transition states for reactive processes involving transient free radicals in faujasites. On the other hand, there is no single (simple) interpretation of $A'_\mu(T)$ for all three of the Δ_1 ALC resonances found for the C_6H_6Mu radical in NaY, as evidenced by the sharply contrasting temperature dependences seen in Figures 8 and 9. Unknown at present, and clearly required, are the temperature dependences of *all* active normal modes contributing to the hfcs for the C_6H_6Mu radical reported herein.

The strong binding of this radical to the cation is reflected as well in the line shapes for the relevant Δ_1 and Δ_0 resonances, which are essentially symmetric and characteristic of a *static* limit over the whole temperature range (3−322 K) studied. This behavior is in *marked* contrast to D-NMR data for benzene in NaY (and other faujasites) at similar *low* loadings to the present μSR study, where clear evidence for both planar (hexad) rotation, and longer range diffusion are seen. Any similar fast isotropic motion, on a time scale $\ll \tau_{ALC} \sim 50$ ns for C_6H_6Mu, would average the hyperfine anisotropy to zero, causing the disappearance of the Δ_1 resonance. The very fact that these lines are seen, even above room temperature, means there can be no such fast isotropic motion. We were nevertheless surprised to

find as well *no evidence* for even fast *uniaxial* rotation of C_6H_6-Mu in NaY, demonstrated by the largely *static* line shapes seen, and thus suggesting activation barriers $\gg$ 1 kJ/mol for in-plane rotation. The lack of even uniaxial motion may be due to the reduced symmetry of the radical compared with the benzene molecule, which gives rise to higher rotational barriers. It could also be due to a stronger binding to the cation,[67] made possible by the open shell structure of the radical in which the partially occupied MO is energetically considerably higher than the HOMO of benzene.

The present results for C_6H_6Mu in NaY are also considerably different in comparison with other μSR data in zeolites, in silicious ZSM-5,[30] and USY,[33] where zero (or reduced) cation concentrations allow much more motion and large deviations from static line shapes are seen over a comparable range of temperatures. They also appear to stand in sharp contrast to one other TF-μSR (only) study on NaX and related faujasites, near or above saturation loadings, where evidence for long-range motion has been reported.[36] This could be a loading dependence, where guest−guest interactions are much more important or the result of additional Na cation sites being accessible to benzene in NaX.

We conclude that the C_6H_6Mu radical at the (S_{II}) Na cation site in NaY is essentially "*frozen*" (on the $\approx$50 ns time scale of the μSR-ALC experiment). There may be some small amplitude motion contributing to slightly narrower lines at the higher temperatures, but of insufficient amplitude to alter the static line shapes. This unexpected result in comparison with other data in turn suggests that Na-cations in NaY act as effective *traps* for cyclohexadienyl radicals, at least at early times and for temperatures near ambient and below. While there may be slightly more motion of the radical at the W site, manifest by the somewhat narrower lines seen at higher temperatures (Table 1), this too is insufficient to appreciably alter the static line shapes seen.

The next phase of this work will be to complete an investigation of this same radical at higher loadings in NaY as well as in other cation-exchanged Y-faujasites, to learn more about the interaction of C_6H_6Mu with different cations in the same cage. It is well-known that changing the alkali cation can have a marked effect on Bronsted acidity,[78] and one may expect similar effects in the binding of the C_6H_6Mu radical to different cations. In addition to examining other framework structures by both TF-μSR and ALC-μSR (including HX, HY, and NaX), and/or different cation environments, it is clearly also of interest to look at other adsorbed molecules and hence different Mu-radicals, with correspondingly different binding and activation energies, by these techniques. To date the vast bulk of free radical studies in zeolites by μSR has been for the cyclohexadienyl radical, as has largely been the case for benzene itself, by NMR, MDS and other techniques.[5] Extending the "parent" benzene molecule to its different xylene derivatives could be a first step, allowing the possibility of seeing more hindered interactions. Another comparison that could be of interest in comparison with the present study of benzene would be to examine cyclohexene, which exhibits no π electron delocalization and can be expected to bind less strongly to cations. Finally, it is certainly of considerable importance to extend these μSR studies to higher temperatures, approaching those of catalytic conditions ($\gtrsim$500 K), where we can expect to see dramatic changes in line widths and shapes as molecular motion becomes more facile.

Acknowledgment. We thank Chemie Uetikon AG of Switzerland for generously providing us with zeolite samples. We also acknowledge both the interest of Dr. Syd Kreitzman in this work and his management of the μSR Facility at TRIUMF and in particular the excellent technical support he provided, along with Curtis Ballard and Mel Good at various stages of this experiment. We also gratefully acknowledge the financial support from the Natural Sciences and Engineering Council (NSERC) of Canada. We also thank Prof. Brian Webster (University of Glasgow) and Dr. Rod Macrae (Radiation Laboratory, Notre Dame) for many helpful (e-mail) discussions and particularly Dr. Macrae for supplying Figure 7, adapted from the calculations of ref 67. One of us (D.G.F.) also thanks the Alexander Von Humboldt Foundation for its awarding of a research prize, facilitating collaborative research both on gas-phase Mu reactivity and on Mu-radicals in zeolites, carried out at the Institute of Physical Chemistry, Universität Stuttgart.

References and Notes

(1) Breck, D. W. *Zeolite Molecular Sieves*; Robert Krieger Publishing: 1973.

(2) Meier, W. M.; Olson, D. H.; Baerlocher, Ch. In *Atlas of Zeolite Structure Types*; Elsevier: Amsterdam, 1996.

(3) Kärger, J.; Ruthven, D. M. *Diffusion in Zeolites and Other Microporous Solids*; Wiley: New York, 1992; Karge, H. G. In *Introduction to Zeolite Science and Practice*; van Bekkum, H., et al., Eds; Elsevier: New York, 1991; p 531.

(4) Catlow, C. R. A. In *Modelling of Structure and Reactivity in Zeolites*; AP: London, 1992.

(5) Barthomeuf, D. *Catal. Rev.* **1996**, *38*, 521.

(6) Kärger, J.; Pfeifer, H. *Zeolites* **1987**, *7*, 90.

(7) Venuto, P. B. In *Progress in Zeolites and Microporous Materials*; Chon, H., et al., Eds.; *Stud. Surf. Sci. Catal*. **1997**, *105*, 811; Jacobs, A.; Martens, J. A. In *Introduction to Zeolite Science and Practice*; van Bekkum, H., et al., Eds.; Elsevier: Amsterdam, 1991; pg 45.

(8) Sastre, G.; Richard, C.; Catlow, A.; Corma, A. *J. Phys. Chem. B* **1999**, *103*, 5187; Sastre, G.; Richard, C.; Catlow, A.; Chica, A.; Corma, A. *J. Phys. Chem. B* **2000**, *104*, 416.

(9) Fuchs, A. H.; Cheetham, A. K. *J. Phys. Chem. B* **2001**, *105*, 7375.

(10) Lange, J.-P.; Gutsze, A.; Karge, H. G. *J. Catal.* **1988**, *114*, 136.

(11) Jockusch, S.; Hirano, T.; Liu, Z.; Turro, N. J. *J. Phys. Chem. B* **2000**, *104*, 1212.

(12) Ottaviani, M. F.; Lei, X.-G.; Liu, Z.; Turro, N. J. *J. Phys. Chem. B* **2001**, *105*, 7954; and references therein.

(13) Werst, D. W.; Han, P.; Chousse, S. C.; Vinokur, E. I.; Xu, L.; Trifunic, A. D.; Erikson, L. A. *J. Phys. Chem. B* **1999**, *103*, 9219.

(14) Harvey, G.; Prins, R.; Crockett, R.; Roduner, E. *J. Chem. Soc., Faraday Trans.* **1996**, *92*, 2027.

(15) Rhodes, C. J.; Hinds, Ch. S. In *Radicals on Surfaces*; Lund, A., Rhodes, C., Eds.; Kluwer: Dordrecht, 1995; p 119.

(16) Lakshminarasimhan, P.; Thomas, K. J.; Bracnceleon, L.; Wood, P. D.; Johnston, L. J.; Ramamurthy, V. *J. Phys. Chem. B* **1999**, *103*, 9247.

(17) Piocos, E. A.; Han, P.; Werst, D. W. *J. Phys. Chem.* **1996**, *100*, 7191.

(18) Kaprinidis, N. A.; Landis, M. S.; Turro, N. J. *Tetrahedron Lett.* **1997**, *38*, 2609.

(19) Doetschman, D. C.; Gilbert, D. C.; Dwyer, D. W. *Chem. Phys.* **2000**, *256*, 37.

(20) Corrent, S.; Martinez, L. J.; Scaiano, J. C.; Garcia, H.; Fornés, V. *J. Phys. Chem. B* **1999**, *103*, 8097; and references therein.

(21) Hill, J.-R.; Freeman, C. M.; Delley, B. *J. Phys. Chem. A* **1999**, *103*, 3772.

(22) Truong, T. N. *J. Phys. Chem. B* **1997**, *101*, 2750.

(23) Czjzek, M.; Fuess, H.; Vogt, T. *J. Phys. Chem.* **1991**, *95*, 5255; Czjzek, M.; Jobic, H.; Bee, M. *J. Chem. Soc., Faraday Trans. 1* **1991**, *87*, 3455.

(24) Gener, I.; Ginestet, G.; Buntinx, G.; Brémard, C. *J. Phys. Chem. B* **2000**, *104*, 11656.

(25) Fleming, D. G.; Arseneau, D. J.; Pan, J. J.; Shelley, M. Y.; Senba, M.; Percival, P. W. *Appl. Magn. Reson.* **1997**.

(26) Roduner, E. *Chem. Soc. Rev.* **1993** p 337.

(27) Roduner, E.; *The Positive Muon as a Probe in Free Radical Chemistry, Lecture Notes in Chemistry, 49*; Springer-Verlag: Berlin Heidelberg, 1988**.**

(28) Yu, D.; Percival, P. W.; Brodovitch, J.-C.; Leung, S.-K.; Kiefl, R. F.; Venkatesvaran, K.; Cox, S. F. J. *Chem. Phys.* **1990**, *142*, 229.

(29) Roduner, E. *Hyperfine Interact.* **1990**, *65*, 857; Roduner, E.; Reid, I. D.; Ricco, M.; De Renzi, R. *Ber. Bunsen-Ges. Phys. Chem.* **1989**, *93*, 1194.

(30) Roduner, E.; Stolmár, M.; Dilger, H.; Reid, I. D. *J. Phys. Chem.* **1998**, *102*, 7591.
(31) Roduner, E. *Appl. Magn. Reson.* **1997**, *13*, 1.
(32) Fleming, D. G.; Shelley, M.; Arseneau, D. J.; Senba, M.; Pan, J. J.; Kreitzman, S. R.; Roduner, E. *Physica B* **2000**, *289*−*290*, 603.
(33) Shelley, M.; Arseneau, D. J.; Senba, M.; Pan, J. J.; Snooks, R.; Kreitzman, S. R.; Fleming, D. G.; Roduner, E. *Stud. Surf. Sci. Catal*. **1994,** *94*, 469.
(34) Blanco, C.; Saravan, C.; Allen, M.; Auerbach, S. M. *J. Chem. Phys.* **2000**, *113*, 9778; Saravan, C.; Auerbach, S. M. *J. Chem. Phys.* **1999**, *110*, 11000; Saravan, C.; Auerbach, S. M. *J. Chem. Phys.* **1998**, *109*, 8755; Saravanan, C.; Jousse, F.; Auerbach, S. M. *J. Phys. Chem.* **1998**, *108*, 2162.
(35) Stolmár, M.; Roduner, E. *J. Am. Chem. Soc*. **1998**, *120*, 583; Stolmár, M.; Roduner, E.; Dilger, H.; Himmer, U.; Shelley, M.; Reid, I. D. *Hyperfine Interact.* **1997**, *106*, 51.
(36) Rhodes, C. J.; Butcher, E. C.; Morris, H.; Reid, I. D. *Magn. Reson. Chem.* **1995**, *33*, 8134.
(37) Rhodes, C. J.; Dintinger, T. C.; Scott, C. A. *Magn. Reson. Chem.* **2000**, *38*, 62.
(38) Roduner, E.; Schwager, M.; Tregenna-Piggott, P.; Dilger, H.; Shelley, M.; Reid, I. D. *Ber. Bunsen-Ges. Phys. Chem.* **1995**, *99*, 1338.
(39) Klein, H.; Kirschhock, C.; Fuess, H. *J. Phys. Chem.* **1994**, *98*, 12345.
(40) Vitale, G.; Bull, L. M.; Morris, R. E.; Cheetham, A. K.; Toby, B. H.; Coe, C. G.; MacDougal, J. E. *J. Phys. Chem.* **1995**, *99*, 16087.
(41) Jobic, H.; Fitch, A. N.; Combert, J. *J. Phys. Chem. B* **2000**, *104*, 8491.
(42) Fitch, A. N.; Jobic, H.; Renouprez, A. *J. Phys. Chem.* **1986**, *90*, 1311.
(43) Bull, L. M.; Henson, N. J.; Cheetham, A. K.; Newsam, J. M.; Heyes, S. J.; et al. *J. Phys. Chem.* **1993**, *97*, 11726.
(44) Isfort, O.; Boddenberg, B.; Fujara, F.; Grosse, R. *Chem. Phys. Lett.* **1998**, *288*, 71.
(45) Boddenberg, B.; Burmeister, R. *Zeolites* **1988**, *8*, 488.
(46) Sousa Goncalves, J. A.; Portsmouth, R. L.; Alexander, P.; Gladden, L. F. *J. Phys. Chem.* **1995**, *99*, 3317.
(47) Chen, Y.-H.; Hwang, L.-P. *J. Phys. Chem.* **1999**, *103B*, 5070.
(48) Klein, H.; Fuess, H.; Schrimpf, G. *J. Phys. Chem.* **1996**, *100*, 11101.
(49) Auerbach, S. M.; Hensen, N. J.; Cheetham, A. K.; Metiu, H. I. *J. Phys. Chem.* **1995**, *99*, 10600; Auerbach, S. M. *J. Chem. Phys.* **1997**, *106*, 7810. 50.
(50) Jousee, F.; Vercouteren, D. P.; Auerbach, S. M. *J. Phys. Chem. B* **2000**, *104*, 8768.
(51) Demontis, P.; Yashonath, S.; Klein, M. L. *J. Phys. Chem.* **1989**, *93*, 5016.
(52) Mossel, T.; Schrimpf, G.; Brickmann, J. *J. Phys. Chem. B* **101 1997**, *9485*, 9476.
(53) Vitale, G.; Mellot, C. F.; Bull, L. M.; Cheetham, A. K. *J. Phys. Chem. B* **1997**, *101*, 4559.
(54) Zhu, L.; Seff, K. *J. Phys. Chem. B* **1999**, *103*, 9512; Zhu, L.; Seff, K.; Olson, D. H.; von Dreek, R. B.; *ibid*, 10365.
(55) Buttefy, S.; Boutin, A.; M.-Draznieks, C.; Fuchs, A. H. *J. Phys. Chem. B* **2001**, *105*, 9569.
(56) Turner, R. E.; Snider, R. F. *Phys. Rev. A* **1998**, *58*, 4431; *Phys. Rev. A* **1996**, *54*, 4815.
(57) Fleming, D. G.; Pan, J. J.; Senba, M.; Arseneau, D. J.; Kiefl, R. F.; Shelley, M. Y.; Cox, S. F. J.; Percival, P. W.; Brodovitch, J.-C. *J. Chem. Phys.* **1996**, *105*, 7517.
(58) Heming, M.; Roduner, E. *Surf. Sci.* **1987**, *189/190*, 535; Heming, M. *Z. Phys. Chem.* **1987**, *151*, 35.
(59) Dilger, H.; Roduner, E.; Stolmár, M.; Reid, I. D.; Fleming, D. G.; Arseneau, D. J.; Pan, J. J.; Senba, M.; Shelley, M. *Hyperfine Interact.* **1997**, *106*, 137.
(60) Roduner, E. *Chem. Phys. Lett.* **1981**, *81*, 191.
(61) Kreitzman, S. R.; Roduner, E. *Chem. Phys.* **1995**, *192*, 189; Kreitzman, S. R. *Chem. Phys.* **1991**, *154*, 353.
(62) Burmeister, R.; Schwarz, H.; Boddenberg, B. *Ber. Bunsen-Ges. Phys. Chem.* **1989**, *93*, 1309; Boddenberg, B.; Beerwerth, B. *J. Phys. Chem.* **1989**, *93*, 1435.
(63) Kiefl, R. F.; Kreitzman, S.; Celio, M.; Keitel, R.; Luke, G. M.; Brewer, J. H.; Noakes, D. R.; Percival, P. W.; Matsuzaki, T.; Nishiyama, K. *Phys. Rev. A* **1986**, *34*, 681.
(64) There are in fact *four* distinct $\Delta M = 0$ resonances seen for C_6H_6-Mu in both the gas[25] and liquid[28,63] phases, corresponding to the four sets of protons at the methylene or ipso (carbon 6), ortho (1, 5), meta (2, 4), and para (3) positions. The methylene resonance is always the strongest in the bulk phase and it is only this resonance that is considered in the present study. In zeolite environments, the much weaker ortho and para resonances for C_6H_6Mu have also been seen in a study of siliceous ZSM-5[30].
(65) The widths reported here are 2σ values from the Gaussian fits, such that the fwhm $= 2.35\sigma$.
(66) Chmelka, B. F.; Pearson, J. G.; Liu, S. B.; Ryoo, R.; de Menorval, L. C.; Pines, A. *J. Phys. Chem.* **1991**, *95*, 303.
(67) Webster, B.; Macrae, R. M. *Physica B* **2000**, *289*−*290*, 598; and private communications.
(68) Chipman, D. M. *J. Phys. Chem.* **1992**, *96*, 3294.
(69) Perera, S. A.; Salemi, L. M.; Bartlett, R. J. *J. Chem. Phys.* **1997**, *106*, 4061.
(70) We had first considered that peak "C" could be the Δ_0 resonance corresponding to the Δ_1 "D" line and suggested this as a possibility in ref 32, but guidance provided now for this Δ_0 resonance from the calculations of Webster and Macrae[67] (Table 2) strongly support the assignment herein of peak "C" as a Δ_1 resonance at the window site.
(71) Weltner, W. *Magnetic Atoms and Molecules*; Dover Publications: Mineola, NY, 1983.
(72) Percival, P. W.; Brodovitch, J.-C.; Leung, S.-K.; Yu, D.; Kiefl, R. F.; Garner, D. M.; Arseneau, D. J.; Fleming, D. G.; Gonzalez, A.; Kempton, J. R.; Senba, M.; Venkateswaran, K.; Cox, S. F. J. *Chem. Phys. Lett.* **1989**, *163*, 241.
(73) Webster, B.; Buttar, D. *J. Chem. Soc., Faraday Trans.* **1996**, *92*, 2231.
(74) Kira, M.; Sugiyama, H.; Sakurai, H. *J. Am. Chem. Soc.* **1983**, *105*, 6436; Kira, M.; Sakurai, H. *J. Am. Chem. Soc.* **1977**, *99*, 3892.
(75) Su, X.; Kung, K.; Laihtinen, J.; Shen, Y. R.; Somorjai, G. A. *Catal. Lett.* **1998**, *54*, 9; and *J. Mol. Catal.***1999**, *A141*, 9.
(76) Voss, V.; Boddenberg, B. *Surf. Sci.* **1993**, *298*, 241.
(77) Schrimf, G.; Tavitian, B.; Espinat, D. *J. Phys. Chem.* **1995**, *99*, 10932.
(78) Vayssilov, G. N.; Rösch, N. *J. Phys. Chem. B* **2001**, *105*, 4277.